# Interband electronic Raman scattering in $p$-silicon

M. A. Kanehisa, R. F. Wallis,* and M. Balkanski
*Laboratoire de Physique des Solides associé au Centre National de la Recherche Scientifique, Université Pierre et Marie Curie, 4, Place Jussieu, 75230 Paris, France*
(Received 23 November 1981)

The electronic Raman scattering efficiency for interband transitions between valence-band states of $p$-type silicon is calculated taking into account the detailed band structure. In contrast to the isotropic model, the real spectrum reflects the band anisotropy: the spectrum extends from zero to rather large scattering frequency with a long tail; there appears a peak at about 500–600 $cm^{-1}$. The result is compared with the experiment of Jouanne and is found to be in fair agreement.

## I. INTRODUCTION

The inelastic scattering of light (Raman scattering) in solids can arise through a number of processes including scattering by elementary excitations such as plasmons, phonons, and magnons. A process which has received relatively little attention is scattering by interband electronic transitions.[1] Several years ago this effect was investigated theoretically[2–7] for semiconductors and semimetals. However, detailed calculations taking into account the actual complexity of the energy-band structure of real solids have not, to our knowledge, been carried out.

Only a few experiments have been done on interband electronic Raman scattering, and they, for the most part, concern intervalence-band scattering in $p$-type silicon.[1,8–11] These experiments have been carried out on rather heavily doped samples in which the continuum of intervalence-band electronic excitations overlaps the Raman-active phonon energy. As a result of this overlap, interference effects appear in the Raman spectrum which cause the latter to become more complicated than is predicted by the simple theory.[3–6]

In order to gain a full understanding of the intervalence-band electronic Raman scattering in $p$-type silicon, it is important to have available the theoretical Raman spectrum associated with intervalence-band transitions when interference effects are absent. This problem may be referred to as the "zero-order" approximation to the more complicated interference problem and enters into the formulation of the latter.[9,12] In this paper, we present a detailed theoretical calculation of the spectrum of the intervalence-band electronic Raman scattering in $p$-type silicon and compare the results with available experimental data.

## II. LIGHT SCATTERING CROSS SECTION FROM BLOCH ELECTRONS

We consider a light scattering process $q \rightarrow q'$, where $q=(\vec{e},\omega,\vec{q})$ ($\vec{e}$, $\omega$, and $\vec{q}$ are the polarization, frequency, wave vector, respectively); here and henceforth unprimed and primed quantities refer to incident and scattered light, respectively. In the case of the scattering of light by noninteracting Bloch electrons, the differential cross section per unit frequency shift $\Omega=\omega-\omega'$ per unit solid angle $o'$ is given by[13]

$$\frac{d^2\sigma}{d\Omega do'}=(n'+1)r_e^2\frac{\omega'}{\omega}\sum_{\alpha,\alpha'}|S_{\alpha'\alpha}(q',q)+R_{\alpha'\alpha}(q',q)|^2(1-f_{\alpha'})f_\alpha\hbar\delta(\hbar\Omega+E_\alpha-E_{\alpha'})\ . \tag{1}$$

Here $\alpha,\alpha'$ refer to one-particle electronic states, $\alpha=(l,s,\vec{k})$ ($l$, $s$, and $\vec{k}$ are the band index, spin index, crystal momentum, respectively) with energy $E_\alpha$ and wave function $u_\alpha \equiv |\alpha)$; $n'$ is the number of scattered photons, which we can take to be zero (spontaneous Raman process); $r_e$ is the classical electron radius; $f_\alpha=f(E_\alpha)$ is the Fermi distribution function; $S$ and $R$ are scattering amplitudes due, respectively, to the $A^2$ term and the $\vec{p}\cdot\vec{A}$ term in the electron-light interaction (see Fig. 1) and are given by

$$S_{\alpha'\alpha}(q',q)=(\vec{e}\,'\cdot\vec{e})(\alpha'|1_{-\vec{Q}}|\alpha)\ , \tag{2}$$

 

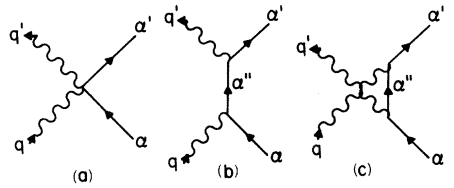


FIG. 1. Light scattering processes from Bloch electrons. An incident photon $q$ is scattered into $q'$. Here $\alpha,\alpha',\alpha''$ refer to electronic states. (a): from the $A^2$ term, giving amplitude $S$; (b) and (c): from the second-order perturbation of the $\vec{p}\cdot\vec{A}$ term in the electron-light interaction, giving two terms in the amplitude $R$.

$$R_{\alpha'\alpha}(q',q)=\frac{1}{m}\sum_{\alpha''}\left[\frac{(\alpha'\mid\Pi'_{\vec{q}'}\mid\alpha'')(\alpha''\mid\Pi_{-\vec{q}}\mid\alpha)}{E_\alpha-E_{\alpha''}+\hbar\omega}+\frac{(\alpha'\mid\Pi_{-\vec{q}}\mid\alpha'')(\alpha''\mid\Pi'_{\vec{q}'}\mid\alpha)}{E_\alpha-E_{\alpha''}-\hbar\omega'}\right], \tag{3}$$

where $m$ is the free-electron mass, $\vec{Q}=\vec{q}-\vec{q}\,'$ is the wave-vector shift, $\Pi=\vec{\Pi}\cdot\vec{e}$, $\Pi'=\vec{\Pi}\cdot\vec{e}\,'$, $(\alpha'\mid O_{\vec{q}}\mid\alpha)$ with $O=1,\Pi,\Pi'$ is the abbreviation of

$$(\alpha'\mid O_{\vec{q}}\mid\alpha)=\int d^3r\, e^{-i\vec{q}\cdot\vec{r}}u^*_{\alpha'}(r)Ou_\alpha(r)\,, \tag{4}$$

and $\vec{\Pi}$ is the momentum operator including the spin-orbit contribution,

$$\vec{\Pi}=\vec{p}+\frac{\hbar}{4mc^2}\vec{\sigma}\times\vec{\nabla}V+\frac{i}{2}\vec{p}\times\vec{\sigma}\,,$$

the last term of which is negligibly small and discarded.

The calculation in our case hence reduces to the computation of $S$ and $R$. Now, since the photon wave vectors $q,q'$ usually are small ($\sim10^4$ cm$^{-1}$ for $\omega\sim2.5$ eV) compared to the Brillouin-zone size ($\sim10^8$ cm$^{-1}$), we can assume "vertical transitions," i.e., set $\vec{q},\vec{q}\,'=0$ in (4), and hence in (2) and (3). Then we only need to evaluate $S$ and $R$ for states $\alpha,\alpha',\alpha''$ with the same crystal momentum $\vec{k}$. Therefore if one writes $n=(l,s)$ then

$$\frac{d^2\sigma}{d\Omega do'}=r_e^2\frac{\omega'}{\omega}\sum_{n,n'}\sum_{\vec{k}}\mid S_{n'n}+R^{\vec{k}}_{n'n}\mid^2\times(1-f_{n'\vec{k}+\vec{Q}})f_{n\vec{k}}\,\hbar\times\delta(\hbar\Omega+E_{n\vec{k}}-E_{n'\vec{k}+\vec{Q}})\,, \tag{5}$$

with

$$S_{n'n}(e',e)=(\vec{e}\,'\cdot\vec{e})(n'\vec{k}\mid n\vec{k})=(\vec{e}\,'\cdot\vec{e})\delta_{n'n}\,, \tag{6}$$

$$R^{\vec{k}}_{n'n}(e',e;\omega',\omega)=\frac{1}{m}\sum_{n''}\left[\frac{(n'\vec{k}\mid\Pi'\mid n''\vec{k})(n''\vec{k}\mid\Pi\mid n\vec{k})}{E_{n\vec{k}}-E_{n''\vec{k}}+\hbar\omega}+\frac{(n'\vec{k}\mid\Pi\mid n''\vec{k}\mid\Pi'\mid n\vec{k})}{E_{n\vec{k}}-E_{n''\vec{k}}-\hbar\omega'}\right]. \tag{7}$$

We note that the amplitude $S$ is nonvanishing only for intraband transitions ($n'=n$), while $R$ can have intra- ($n'=n$) as well as interband ($n'\neq n$) contributions. In this paper we are mainly concerned with the interband excitations.

A simplified analysis assuming isotropic parabolic energy bands would give an interband spectrum which has zero temperature cutoffs at both the low- and high-frequency shifts,

$$\hbar\Omega_m=[1-(m_l/m_h)]E_F$$

and

$$\hbar\Omega_M=[(m_h/m_l)-1]E_F\,,$$

in view of the excitation process shown in Fig. 2(a), where $m_l$ and $m_h$ are the light- and heavy-hole masses, respectively, and $E_F$ is the Fermi energy.[14] The spectrum is schematically shown in Fig. 2(b). However, as is well known, silicon has highly anisotropic valence bands, and in order to obtain quantitative results a knowledge of the detailed band structure over the whole Brillouin zone is necessary.

## III. INTERBAND RAMAN EFFICIENCY FOR $p$ SILICON

In order to obtain the band structure, we adopt Cardona and Pollak's full-zone $\vec{k}\cdot\vec{p}$ scheme.[15] In the one-electron Schrödinger equation for a state $\mid n\vec{k})$,

$$\left[\frac{1}{2m}\vec{p}^2+V+\frac{\hbar}{4m^2c^2}(\vec{\sigma}\times\vec{\nabla}V)\cdot\vec{p}\right]\mid n\vec{k})=E_{n\vec{k}}\mid n\vec{k})\,,$$

substitution of the Bloch function $\mid nk)=e^{i\vec{k}\cdot\vec{r}}$

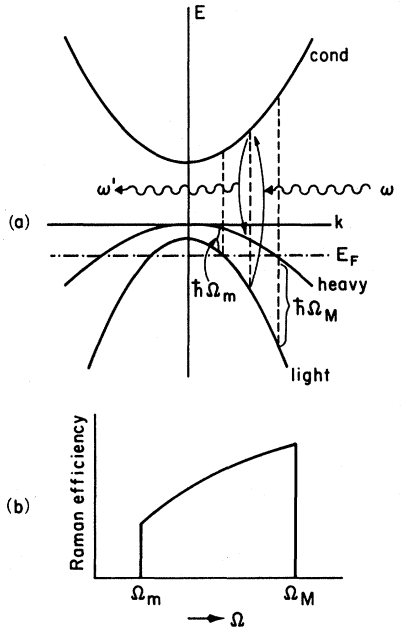


FIG. 2. (a) Isotropic parabolic energy bands with the Fermi energy $E_F$ in the valence bands. Incident light $\omega$ excites from the light-hole band (light) to the conduction band (cond) an electron, which, by emitting a scattered photon $\omega'$, deexcites to the heavy-hole band (heavy), leaving a net transition light→heavy. (b) These intervalence-band transitions give a Raman spectrum with cutoffs at $\Omega_m$ and $\Omega_M$ (schematic).

$\times U_{n\vec{k}}$ gives an equation for the cell-periodic part $U_{n\vec{k}}$:

$$\left[H_0+\frac{\hbar}{m}\vec{k}\cdot\vec{p}+H_{so}\right]U_{n\vec{k}} = \left[E_{n\vec{k}}-\frac{\hbar^2}{2m}k^2\right]U_{n\vec{k}}\,. \quad (8)$$

Here $H_0$ is the Hamiltonian for $\vec{k}=0$ and $H_{so}$ is the spin-orbit interaction

$$H_{so}=\frac{\hbar}{4m^2c^2}(\vec{\sigma}\times\vec{\nabla}V)\cdot(\vec{p}+\hbar\vec{k})\,,$$

whose second term, linear in $\vec{k}$, is much smaller than the $\vec{k}$-independent first term, and is neglected. Since the Bloch functions at $\vec{k}=0$ ($U_{n\vec{k}=0}$) form a complete set of periodic functions, it is possible to expand $U_{n\vec{k}}$ at *any* value of $\vec{k}$ (not only for small $\vec{k}$) in terms of $U_{n\vec{k}=0}$, if enough basis states are taken. Without spin-orbit interaction, Cardona and Pollak take four valence states, $\Gamma_1^l$ and $\Gamma_{25'}^l$, and eleven conduction states, $\Gamma_{15'}$, $\Gamma_{2'}^l$, $\Gamma_{12'}$, $\Gamma_1^u$, $\Gamma_{25'}^u$, and $\Gamma_{2'}^u$, where $l$ (lower) and $u$ (upper) distinguish two different states with the same symmetry. We then need as parameters eight eigenvalues of $H_0$ corresponding to the above states and ten independent matrix elements $(\Gamma\,|\,\vec{p}\,|\,\Gamma')$ of momentum $\vec{p}$ between these states. Diagonalization of a $15\times15$ matrix at any point $\vec{k}$ in the Brillouin zone gives the eigenvalues $E_{n\vec{k}}$ of Eq. (8) and the eigenvectors $C_{n\vec{k}}$ which are the expansion coefficients of $U_{n\vec{k}}$ in terms of $U_{n\vec{k}=0}$ ($U_{n\vec{k}}=\sum_m U_{m\vec{k}=0}\times C_{n\vec{k}}^{(m)}$).

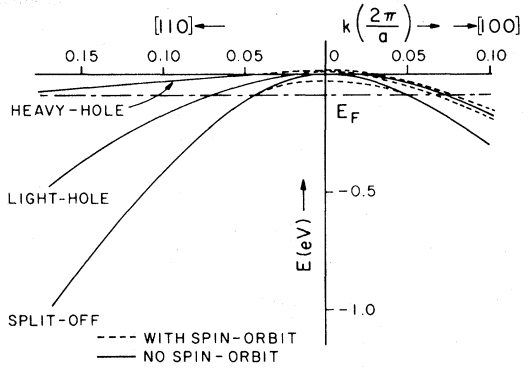


FIG. 3. Silicon valence-band edge calculated by Cardona and Pollak's full-zone $\vec{k}\cdot\vec{p}$ method (Ref. 12) with and without spin-orbit coupling. The Fermi energy $E_F=0.1$ eV corresponds to an acceptor concentration $p\sim10^{20}$ cm$^{-3}$.

The inclusion of the spin-orbit interaction presents no difficulty. We are confronted with additional parameters of the form $(\Gamma\,|\,H_{so}\,|\,\Gamma')$, of which only two are significant: $(\Gamma_{15}\,|\,H_{so}\,|\,\Gamma_{15})$ and $(\Gamma_{25'}\,|\,H_{so}\,|\,\Gamma_{25'})$. One then needs to diagonalize complex $30\times30$ matrices to obtain corresponding energies and wave functions.

Using the parameters for silicon given by Cardona and Pollak,[15] we calculated the energy bands and eigenfunctions. We show in Fig. 3 the valence-band edge of silicon with and without spin-orbit coupling as well as the Fermi level $E_F\sim100$ meV corresponding to an acceptor concentration $p\sim10^{20}$ cm$^{-3}$. First we see that the uppermost band (heavy-hole band) is rather flat in the [110] direction. Hence the region where interband transitions are possible is relatively extended, from $k\sim0.045(2\pi/a)$ to $k\sim0.19(2\pi/a)$. We can expect that this rather large $k$ range should give the Raman spectrum a long tail (up to 1 eV$\sim$8000 cm$^{-1}$). Second, in the [100] and [111] directions (not shown in this figure), the heavy-hole and the light-hole bands are degenerate (without spin-orbit). Therefore the transition between these two bands gives contributions near zero-frequency shift in the

Raman spectra. The third thing that we can say is that the spin-orbit interaction mainly perturbs the states near $\Gamma$ and gives small splittings of the light- and heavy-hole bands in the [100] and [111] directions. The principal effect of including the spin-orbit interaction would be to give low-frequency-shift contributions to the Raman scattering arising from transitions between the split light- and heavy-hole bands. Since our primary interest in this paper is the frequency-shift region above 400 $cm^{-1}$, we neglect the spin-orbit interaction. In a subsequent paper we shall consider the low-frequency-shift region in detail and include the spin-orbit interaction.

We thus calculated without spin-orbit coupling[16] the Raman amplitude (7) as a function of $\vec{k}$ between two valence states $n$ and $n'$, taking all 15 states as intermediate states $n''$. Since there are three valence states, there are three combinations $(n,n')$, of which at $T=0$ two are realized depending on the Fermi level $E_F$. The momentum matrix elements appearing in (7) can be given in terms of $(\Gamma \mid \vec{p} \mid \Gamma')$ as

$$(n\vec{k} \mid \vec{p} \mid n'\vec{k}) = \vec{k}\delta_{nn'} + (U_{n\vec{k}} \mid \vec{p} \mid U_{n'\vec{k}})$$
$$= \vec{k}\delta_{nn'} + \sum_{m,m'} (U_{m\vec{k}=0} \mid \vec{p} \mid U_{m'\vec{k}=0}) \times C^{(m)*}_{n\vec{k}} C^{(m')}_{n'\vec{k}} .$$

An example of the Raman amplitude is shown in Fig. 4 for $n=\Delta_2$ and $n'=\Delta_5$, for incident light $\hbar\omega=2.54$ eV (488 nm) polarized along $y$ and scattered light polarized along $x$. Note that this Raman tensor $R^{\vec{k}}(x,y)$ is fairly dependent on $k$ in the region we are interested in, $k=0-0.4(2\pi/a)$. Integration of this Raman tensor in $\vec{k}$ space [see Eq. (5)] gives the Raman efficiency (cross section divided by crystal volume). The zone integration was carried out by using Gilat's extrapolation method.[17]

Figure 5 shows the calculated Raman spectra at $T=0$ for incident light $\hbar\omega=2.54$ eV (488 nm) polarized along $x$ or $y$, for two concentrations $p=1.13\times10^{20}$ $cm^{-3}$ ($E_F=92$ meV) and $p=1.60\times10^{20}$ $cm^{-3}$ ($E_F=114$ meV). First note that the intensity in the parallel configuration $(x,x)$ is much smaller than in the perpendicular configuration $(x,y)$. This can be explained as follows. The Raman operator $R(e',e)$, $e,e'=x,y,z$ transforms like a tensor of rank two. At $\Gamma$ point ($\vec{k}=0$) valence states are three eigenfunctions of $H_0$ belonging to $\Gamma_{25'}$ ($X$, $Y$, and $Z$). The nonvanishing matrix elements of $R(x,x)$ are

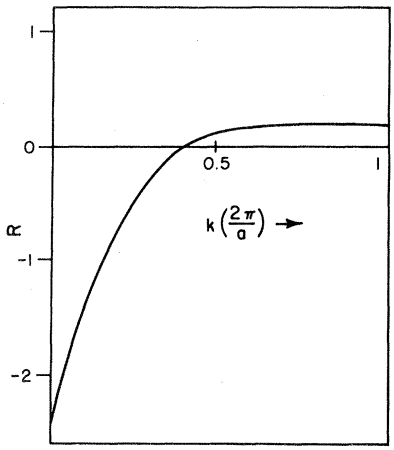


FIG. 4. Raman amplitude $R$ (dimensionless) as a function of $k\|[100]$ between two valence bands $\Delta_5$ and $\Delta_2$, for incident light $\hbar\omega=2.54$ eV polarized along $x$ and scattered light polarized along $y$.

$$(X \mid R(x,x) \mid X) \approx (Y \mid R(x,x) \mid Y) = (Z \mid R(x,x) \mid Z) . \quad (9)$$

As for $R(x,y)$, there are two elements,

$$(X \mid R(x,y) \mid Y) \approx (Y \mid R(x,y) \mid X) .$$

Now for $k\neq0$, if one denotes the direction cosines of $\vec{k}$ as $(a,b,c)$, then one of the valence states

$$\bar{Z} = aX + bY + cZ$$

is lower in energy than almost-degenerate two other states,

$$\bar{X} = a'X + b'Y + c'Z ,$$
$$\bar{Y} = a''X + b''Y + c''Z ,$$

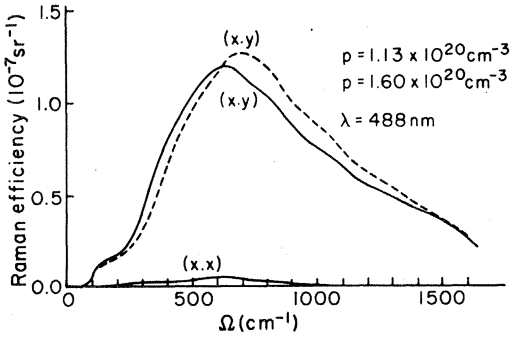


FIG. 5. Calculated interband electronic Raman spectra at $T=0$, for concentrations $p=1.13\times10^{20}$ $cm^{-3}$ (solid curves) and $p=1.60\times10^{20}$ $cm^{-3}$ (dashed curve). Here $(x,x)$ or $(x,y)$ indicates (incident polarization, scattered polarization). Incident light energy is $\hbar\omega=2.54$ eV ($\lambda=488$ nm).

where $(a,b,c)$, $(a',b',c')$, and $(a'',b'',c'')$ are mutually perpendicular. The matrix elements of $R(x,x)$ between $\bar{X}$ and $\bar{Y}$ almost vanish:

$$(\bar{X}\,|\,R(x,x)\,|\,\bar{Y})=a'a''(X\,|\,R(x,x)\,|\,X)+b'b''(Y\,|\,R(x,x)\,|\,Y)+c'c''(Z\,|\,R(x,x)\,|\,Z)\approx 0\ ,$$

because of (9) and similarly ($\bar{X}$ or $\bar{Y}\,|\,R(x,x)\,|\,\bar{Z}$) $\approx 0$, while $R(x,y)$ has nonzero elements for any of two states (except for some symmetry directions). For example,

$$(\bar{X}\,|\,R(x,y)\,|\,\bar{Y})=a'b''(X\,|\,R(x,y)\,|\,X)+a''b'(Y\,|\,R(x,y)\,|\,X)\ .$$

In the perpendicular configuration $(x,y)$, one can clearly see, as expected, the spectra extend from zero to the large-frequency region with a long tail. The spectra have singularities (shoulders) as well as a broad peak at about 560 $\mathrm{cm}^{-1}$. The peak shifts toward high frequencies when one increases the concentration. These features can be interpreted by the following phase space arguments (see Fig. 6). The transition $n\rightarrow n'$ is possible in the $\vec{k}$ space only where the condition $E_{n\vec{k}}<E_F<E_{n'\vec{k}}$ is satisfied. If the matrix elements are assumed constant, the cross section $d\sigma(\Omega)/d\Omega$ is proportional to the area of the surface

$$\hbar\omega_{n'n}(\vec{k})\equiv E_{n'\vec{k}}-E_{n\vec{k}}=\hbar\Omega$$

contained in the above region. The shoulders are due to the anisotropic forms of the valence bands. If one increases the concentration, the Fermi surfaces $E_{n\vec{k}}=E_F$ displace outward and the surfaces $\omega_{n'n}(\vec{k})=\Omega$ with larger $\Omega$ will be included in the region $E_{n\vec{k}}<E_F<E_{n'\vec{k}}$ hence the displacement of the peak toward high $\Omega$. This analysis combined with experimental information about peaks and shoulders by changing the concentrations might give insight into the valence-band structure away from the $\Gamma$ point.

Finally, Fig. 7 shows the Raman intensity at the peak for a given concentration as a function of incident-light energy. One can clearly see the resonance behavior: The intensity increases as the incident-light energy approaches the energy gap 3.3 eV. This behavior is well approximated[9] by the inverse-energy rule $(E_g-\hbar\omega)^{-1}$, obtained by taking into account only the one-dimensional critical point $E_0'$ at 3.3 eV.

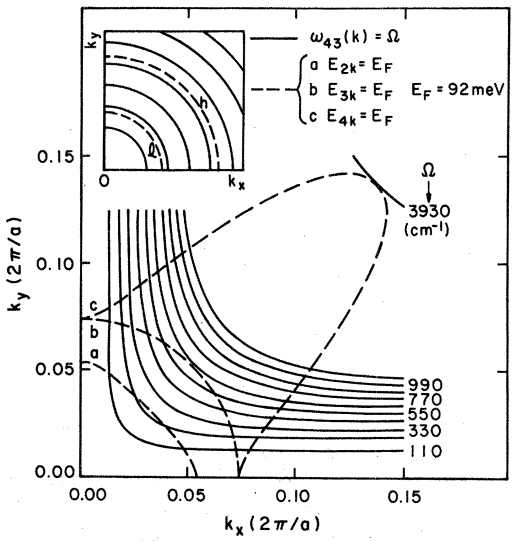


FIG. 6. Phase-space analysis. Inset: Isotropic band model of Fig. 2(a). The (001) section of surfaces of constant energy difference $\omega_{hl}(\vec{k})=\Omega$ (where $\hbar\omega_{hl}\equiv E_{h\vec{k}}-E_{l\vec{k}}$) for various $\Omega$ (solid curves) as well as two Fermi surfaces $E_{l\vec{k}}=E_F$ ($l$ indicates light hole) and $E_{h\vec{k}}=E_F$ ($h$ indicates heavy hole) (dashed curves) are shown. The interband transition $l\rightarrow h$ is possible in the hatched region where $E_{l\vec{k}}<E_F<E_{h\vec{k}}$. If the Raman matrix elements are assumed constant, the cross section at $\Omega$, $d\sigma(\Omega)/d\Omega$, is proportional to the area of the surface $\omega_{hl}(\vec{k})=\Omega$, and one obtains the spectrum of Fig. 2(b). Main figure: In real silicon, essentially the same arguments hold. Here one has three Fermi surfaces (dashed curves), (a) $E_{2\vec{k}}=E_F$, (b) $E_{3\vec{k}}=E_F$, and (c) $E_{4\vec{k}}=E_F$ as well as three sets of surfaces $\omega_{43}(\vec{k})=\Omega$, $\omega_{32}(\vec{k})=\Omega$, and $\omega_{42}(\vec{k})=\Omega$, of which only the first set is shown in this figure (solid curves with $\Omega$ values in $\mathrm{cm}^{-1}$). The interband transitions $3\rightarrow 4$ are possible only for those parts of surfaces $\omega_{43}(k)=\Omega$ that are included by two Fermi surfaces $b$ and $c$ where the condition $E_{3\vec{k}}<E_F<E_{4\vec{k}}$ is satisfied. This gives the long-tailed spectra as shown in Fig. 5.

## IV. COMPARISON WITH EXPERIMENT AND DISCUSSION

Figure 8 shows Jouanne's experimental Raman spectrum[18] of silicon doped with boron $^{10}$B with a concentration $p=1.13\times 10^{20}$ $\mathrm{cm}^{-3}$ at $T=2$ K as well as our calculated electronic Raman spectrum corresponding to the same concentration at $T=0$ K. Since it is difficult to obtain experimentally the absolute intensity, we fitted the value at $\Omega=1150$ $\mathrm{cm}^{-1}$ (see below). The experimental spectrum has various phonon contributions: The peak near

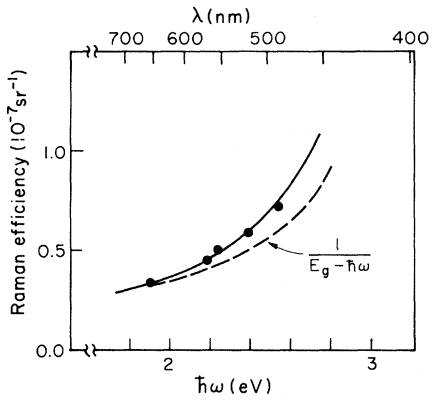


FIG. 7. Resonance spectrum. Solid curve: calculated result for the Raman peak intensity at $T=0$ as a function of incident light energy $\hbar\omega$ for a given concentration $p=1.13\times10^{20}$ cm$^{-3}$ with $E_F=92$ meV. Dashed curve: contribution only from the one-dimensional singularity $E_0'$ would give the $(E_g-\hbar\omega)^{-1}$ behavior. Closed circles: Experimental results (Ref. 15) ($T=2$ K) at $\Omega=200$ cm$^{-1}$. The value at $\hbar\omega=1.92$ eV ($\lambda=647$ nm) was fitted to the calculated absolute value.

$\Omega=520$ cm$^{-1}$ is due to the zone-center optical phonons and the peak at 642 cm$^{-1}$ is the $^{10}$B localized mode, both interfering with the electronic continuum.[8–11] The band at 950 cm$^{-1}$ is the contribution of two zone-edge TO phonons.[19] There is also a two-phonon background,[19] extending up to $\Omega=2\omega_{LO}=1040$ cm$^{-1}$, whose contribution is seen at the antiresonance frequency $\Omega\approx460$ cm$^{-1}$, where otherwise the intensity should vanish. The spectrum for $\Omega>1040$ cm$^{-1}$ is purely electronic and in fact the agreement with theory is satisfactory.

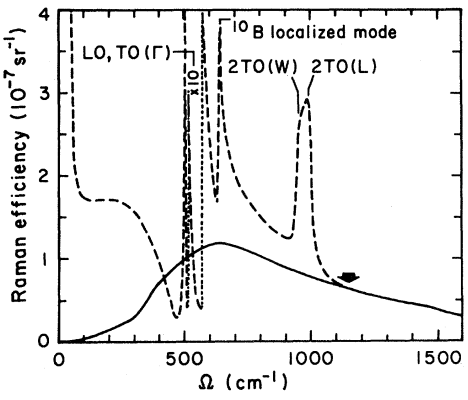


FIG. 8. Solid curve: calculated electronic Raman spectrum at $T=0$ in $(x,y)$ configuration. Dashed curve: experimental Raman spectrum (Ref. 15) for $^{10}$B-doped silicon at $T=2$ K; [111] incidence, back scattering, polarization not analyzed. Both spectra for a concentration $p=1.13\times10^{20}$ cm$^{-3}$ ($E_F=92$ meV), and incident light $\hbar\omega=2.54$ eV ($\lambda=488$ nm). Absolute experimental value was obtained by comparing the value at $\Omega=1150$ cm$^{-1}$ (indicated by an arrow) with theory. Various phonon contributions are indicated.

Apart from the interference region, whose detailed analysis has appeared elsewhere,[20] there is a large discrepancy at low frequencies ($\Omega\lesssim400$ cm$^{-1}$). The experimental spectrum near $\Omega=0$ contains stray laser light (up to 80 cm$^{-1}$ according to Ref. 18). The intraband transitions might contribute to quasielastic scattering but this extends only to $\Omega\sim Qv_F\sim200$ cm$^{-1}$ ($Q$ indicates wave-vector transfer as before, and $v_F$ is the Fermi velocity), and further these single-particle excitations are heavily screened by a factor $(Q/q_{TF})^4\sim(\frac{1}{500})^4$ ($q_{TF}$ is the Thomas-Fermi screening wave vector).[1] Hence it is somewhat difficult to explain this rather large intensity at low frequencies. The spin-orbit interaction would give rise to two effects. First, the threshold of the intervalence-band transitions is displaced by a frequency corresponding to heavy-light splitting at the Fermi level of the highest valence band in [100] and [111] directions (see Fig. 3), which is typically of order of 250 cm$^{-1}$. The second effect is the contribution from spin-density fluctuations in the intraband transitions,[1] which are not screened, and might explain the behavior for $\Omega\lesssim Qv_F$. Detailed analysis of this low-frequency region will be the subject of future investigations.

In view of the strong screening effects on intraband scattering, one may ask whether screening has significant effects on interband scattering. This question has been addressed by Mills *et al.*[4] who find that the effect of electron-electron interactions is small when the carrier concentration is large ($>10^{14}$ holes/cm$^3$), as is assumed in the present paper.

In Fig. 7, our resonance curve is compared with experiment.[18] Observed Raman intensities at $\Omega=200$ cm$^{-1}$ are plotted as a function of incident laser energy (closed circles) by fitting the value at $\hbar\omega=1.92$ eV ($\lambda=647$ nm). Experimental resonance behavior is well explained by our theory.

Finally we note that the calculated electronic intensity furnishes a reference to obtain absolute phonon intensities. For instance, from the spectrum of Fig. 8, we get the total 2 TO efficiency $1.22\times10^{-5}$ cm$^{-1}$ sr$^{-1}$.

## ACKNOWLEDGMENTS

We would like to thank Professor L. M. Falicov for encouraging discussions and many helpful remarks, particularly regarding the selection rules. We are grateful to Dr. M. Jouanne for discussions of the experimental data prior to publication. Research for one of us (R. F. W.) was supported in part by NSF Grant No. DMR-7809430.

---

*Permanent address: University of California, Irvine, California 92717.

[1]See for review, M. V. Klein, in *Light Scattering in Solids,* edited by M. Cardona (Springer, Berlin, 1975), p. 147.

[2]A. A. Grinberg, Fiz. Tekh. Polaprovodn. 2, 1265 (1969) [Sov. Phys.—Semicond. 2, 1018 (1969)].

[3]E. Burstein, D. L. Mills, and R. F. Wallis, Phys. Rev. B 4, 2429 (1971).

[4]D. L. Mills, R. F. Wallis, and E. Burstein, in *Light Scattering in Solids,* edited by M. Balkanski (Flammarion, Paris, 1971), p. 107.

[5]G. B. Wright and M. Balkanski, Mater. Res. Bull. 6, 1097 (1971).

[6]S. Srivastava and K. Arya, Phys. Rev. B 8, 667 (1973).

[7]F. Bechstedt, R. Enderlein, and K. Peuker, Phys. Status Solidi (B) 68, 43 (1975).

[8]R. Besermann, M. Jouanne, and M. Balkanski, in *Proceedings of the Eleventh International Conference on the Physics of Semiconductors,* edited by M. Miasek (Polish Scientific, Warsaw, 1972), p. 1181.

[9]M. Balkanski, K. P. Jain, R. Besermann, and M. Jouanne, Phys. Rev. B 12, 4328 (1975).

[10]F. Cerdeira, T. A. Fjeldly, and M. Cardona, Solid State Commun. 13, 325 (1973); Phys. Rev. B 8, 4734 (1973).

[11]F. Cerdeira, T. A. Fjeldly, and M. Cardona, Phys. Rev. B 9, 4344 (1974).

[12]F. Bechstedt and K. Peuker, Phys. Status Solidi B 72, 743 (1975).

[13]See for example, S. S. Jha, Nuovo Cimento 63B, 331 (1969).

[14]R. F. Wallis, lecture notes, Université Pierre et Marie Curie (unpublished).

[15]M. Cardona and F. H. Pollak, Phys. Rev. 142, 530 (1966).

[16]Inclusion of the spin-orbit interaction is only a problem of computation time.

[17]G. Gilat and L. J. Raubenheimer, Phys. Rev. 144, 390 (1966).

[18]M. Jouanne (unpublished).

[19]P. A. Temple and C. E. Hathaway, Phys. Rev. B 7, 3685 (1973).

[20]K. Arya, M. A. Kanehisa, M. Jouanne, K. P. Jain, and M. Balkanski, J. Phys. C 12, 3843 (1979).